Journal of Materials Chemistry B

PAPER

View Article Online
View Journal | View Issue

Cite this: J. Mater. Chem. B, 2014, 2, 6119

Electroactive nanofibrous biomimetic scaffolds by thermally induced phase separation†

Longchao Li,‡[a] Juan Ge,‡[a] Ling Wang,[a] Baolin Guo*[a] and Peter X. Ma*[abcde]

Received 28th March 2014
Accepted 18th July 2014

DOI: 10.1039/c4tb00493k

www.rsc.org/MaterialsB

Fabrication of functional nanofibrous biomimetic scaffolds for tissue regeneration remains a challenge. This work demonstrates that functional nanofibrous scaffolds were fabricated from blends of polylactide with other functional polymers by a thermally induced phase separation (TIPS) technique, here exemplified by the fabrication of electroactive nanofibrous scaffolds from the blends of polylactide and an electroactive degradable tetraaniline–polylactide–tetraaniline (TPT) block copolymer by TIPS. The TPT copolymer was synthesized by coupling reaction between the carboxyl-capped tetraaniline and polylactide. The chemical structure, electroactivity, thermal properties and mechanical properties of TPT and polylactide/TPT blend films were characterized. The copolymer blends were fabricated into electroactive nanofibrous scaffolds by TIPS. The effect of aniline tetramer content, polymer concentration and phase separation temperature on the diameter of nanofibers was investigated. The adhesion and proliferation of C2C12 myoblast cells and protein adsorption on the electroactive biodegradable substrates were evaluated, and the results show that the electroactive materials are nontoxic and could enhance the C2C12 cell proliferation without electrical stimulation, and adsorbed more proteins compared to polylactide. The electrical stimulation on the electroactive substrates significantly increased the cell proliferation of C2C12 myoblasts. This work opens the way to fabricate functional nanofibrous scaffolds from the blends of polylactide and other functional polymers by TIPS.

Introduction

Biomaterials play a pivotal role in tissue healing and regeneration processes. Biodegradable porous scaffolds provide three-dimensional templates which can support cell attachment, proliferation, differentiation and neo tissue genesis.[1–5] It is beneficial for the scaffold as a synthetic temporary extracellular matrix (ECM) to mimic the nanofibrous structure of the natural ECM.[6–9] Biomimetic scaffolds with nanofibrous structure are usually created by electrospinning, self-assembly and a thermally induced phase separation (TIPS) technique.[10–14] With great processing flexibility, TIPS is a promising method to fabricate scaffolds for a wide range of applications in tissue regeneration.[15–17] Most of the work reported the synthesis of nanofibrous scaffolds by TIPS from polylactide and poly(lactide-*co*-glycolide) copolymers.[15] However, polylactide and poly(lactide-*co*-glycolide) copolymers lack bioactivity, and it remains a challenge to fabricate functional nanofibrous biomimetic scaffolds from the blends of polylactide and other functional polymers.

Recent research showed that a range of cellular activities including cell adhesion, proliferation and differentiation were tuned by conducting polymers with electrical stimulations.[18–20] However, the non-degradability and poor processability of conducting polymers greatly restricted their applications in tissue engineering. Nanofibrous conductive scaffolds based on blends of polyaniline or polypyrrole with other degradable polymers were created by electrospinning.[21–23] However, the electrospinning technique usually has some limitations to generate three-dimensional scaffolds with well-defined pore size.[24–26] Furthermore, polyaniline and polypyrrole in the scaffolds are not degradable and expected to stay *in vivo*[21–23,27] even though a small amount of them was used in the blends.[28] Therefore, biodegradable and conductive polymers and their applications as scaffolds for tissue regeneration have gained more and more attention.[19,23] We synthesized a series of degradable conducting polymers[29–31] and hydrogels[32,33] with different macromolecular architectures, moderate

[a]Center for Biomedical Engineering and Regenerative Medicine, Frontier Institute of Science and Technology, Xi'an Jiaotong University, Xi'an, 710049, China. E-mail: baoling@mail.xjtu.edu.cn; mapx@umich.edu; Fax: +86-29-83395131; Tel: +86-29-83395361

[b]Department of Biomedical Engineering, University of Michigan, Ann Arbor, MI 48109, USA

[c]Department of Biologic and Materials Sciences, University of Michigan, 1011, North University Ave., Room 2209, Ann Arbor, MI 48109, USA

[d]Macromolecular Science and Engineering Center, University of Michigan, Ann Arbor, MI 48109, USA

[e]Department of Materials Science and Engineering, University of Michigan, Ann Arbor, MI 48109, USA

† Electronic supplementary information (ESI) available. See DOI: 10.1039/c4tb00493k

‡ These authors contributed equally.

hydrophilicity and tunable conductivity. However, the nanofibrous electroactive degradable scaffolds which could mimic the structure of the natural ECM have not been reported.

The aim of this work is to fabricate electroactive nanofibrous biodegradable scaffolds from the blends of polylactide and an electroactive degradable polymer by a thermally induced phase separation technique. We hypothesize that the nanofibrous structure of the scaffolds could mimic the physical structure of the ECM, while the electroactivity can be used to regulate the cellular activity during tissue regeneration. The synthesis of electroactive degradable block copolymers and the properties of their blends with polylactide including chemical structure, electroactivity, thermal properties, hydrophilicity and mechanical properties were investigated. The fabrication of electroactive nanofibrous scaffolds from the blends by TIPS was studied. The effect of polymer concentration and phase separation temperature on the nanofibrous structure was studied. The good biocompatibility of these scaffolds was investigated by cell adhesion and proliferation of C2C12 myoblasts. This work will open the door for fabrication of various functional nanofibrous scaffolds from the polylactide blends by TIPS.

Experimental

Materials

L-Lactide (LLA, Aldrich) was purified by recrystallization in dry toluene twice and subsequently dried under reduced pressure for 3 days prior to polymerization. Aniline (J&K Scientific Ltd.) was distilled twice under reduced pressure. Stannous octoate, $Sn(Oct)_2$ (Aldrich), was dried over molecular sieves and stored in a glovebox (MBraun labstar) purged with nitrogen. *N*-Phenyl-1,4-phenylenediamine, *p*-phenylenediamine, ammonium persulfate ($(NH_4)_2S_2O_8$), hydrochloric acid (HCl), ethanol (EtOH), dimethyl sulphoxide (DMSO), succinic anhydride (SA), chloroform ($CHCl_3$), ammonium hydroxide (NH_4OH), phenylhydrazine, *N*′-dicyclohexyl carbodiimide (DCC), 4-dimethylaminopyridine (DMAP) and camphorsulfonic acid (C) were all purchased from Aldrich and were used as received.

Synthesis of polylactide with different molecular weights

Linear polylactides (P) with different molecular weights were prepared by ring-opening polymerization (ROP).[34] Briefly, monomer (LLA), catalyst ($Sn(Oct)_2$) and initiator (ethylene glycol (EG)) were weighed and added into a silanized round-bottomed flask in a glovebox filled with nitrogen (MBraun labstar). The flask was then placed in an oil bath at 110 °C for 48 h. After 48 h, 20 mL chloroform was added to dissolve the mixture. The mixture was then precipitated in 200 mL ether. The cake was vacuum dried under room temperature for 2 days after filtration. The theoretical molecular weights of two kinds of linear P were 80k and 1.5k, respectively. Samples were named *e.g.* P80k, meaning polylactide with a molecular weight of 80 000.

Synthesis of tetraaniline

Tetraaniline (T) was synthesized in a two-step reaction. The amino group of *N*-phenyl-1,4-phenylenediamine was firstly protected with butane diacid anhydride in CH_2Cl_2. 0.1 mol carboxyl-capped *N*-phenyl-1,4-phenylenediamine and 0.1 mol *p*-phenylenediamine were dissolved in a mixture solution of DMF and 1 mol L^{-1} hydrochloric acid (HCl) (v/v = 1 : 1). The emeraldine (EM) base form of T was prepared by adding 0.2 mol oxidant ammonium persulfate to the above solution under vigorous stirring for 4 h and dedoped with 1 mol L^{-1} NH_4OH. The fully reduced leucoemeraldine (LM) T was obtained by reducing the EM T with phenylhydrazine. The gray product was finally dried under vacuum for 48 h.

LM T: ^{1}H NMR (400 MHz, DMSO-d_6): δ = 12.05 (s, 1H, –COOH), δ = 9.71 (s, 1H, –NHCO–), δ = 7.76 (s, 1H, –NH–), δ = 7.67 (s, 1H, –NH–), δ = 7.63 (s, 1H, –NH–), δ = 7.36–7.38 (d, 2H, Ar-H), δ = 7.12–7.13 (d, 2H, Ar-H), δ = 6.99–6.86 (m, 12H, Ar-H), δ = 6.69–6.65 (d, 2H, Ar-H), δ = 2.74–2.72 (t, 4H, $-CH_2CH_2-$). ^{13}C NMR (100 MHz, DMSO-d_6) δ = 174.41 (–COOH), 169.73 (–CONH–), 145.87 (Ar-C), 141.08 (Ar-C), 139.14 (Ar-C), 138.00 (Ar-C), 136.59 (Ar-C), 135.32 (Ar-C), 131.32 (Ar-C), 129.52 (Ar-C), 121.08 (Ar-C), 120.91 (Ar-C), 119.71 (Ar-C), 118.67 (Ar-C), 118.37 (Ar-C), 117.90 (Ar-C), 116.01 (Ar-C), 115.03 (Ar-C), 31.33 ($-CH_2-$), 29.44 ($-CH_2-$).

Synthesis of the TPT block copolymer

The schematic routine for the synthesis of the TPT copolymer is shown in Scheme 1. P1.5k (0.001 mol) and T (0.002 mol) were dissolved in 10 mL 1,4-dioxane in a dried flask. DMAP (0.0015 mol) and DCC (0.0025 mol) were then added into the flask after dissolving. The reaction was carried out at room temperature for 72 h. The mixture was then filtered to remove dicyclohexylurea. The filtrate was precipitated in 150 mL ether. The product was finally dried in a vacuum oven for 3 days.

Preparation of electroactive degradable P80k/TPT films

Films of P80k blended with TPT copolymers were fabricated by a solution-casting method. Appropriate amounts of P80k and TPT copolymer as listed in Table 1 were dissolved in THF. The mixture was then cast into a Petri dish, and the solvent was allowed to evaporate in a fume hood for 4 days. The film obtained was dried in a vacuum oven for 3 days. The T content was set as 2 wt%, 5.5 wt% and 9 wt% in the blends. The C doped blends were fabricated in a similar manner except that the various amounts of dopant C (4 wt% of TPT copolymer) were added to the mixture.

Fabrication of P80k/TPT nanofibrous scaffolds by TIPS

Nano-fibrous scaffolds from P80k and P80k/TPT blends were fabricated by employing the thermally induced phase separation technique.[35] Briefly, 3.0 mL polymer solution (7.5 wt% or 5 wt%) in THF was cast into a Teflon vial. The polymer solution was then phase separated at −20 or −80 °C for 4 h and then soaked into distilled water to exchange THF for 2 days. The obtained matrix was freeze-dried for 3 days. The dried porous scaffolds were then stored in a desiccator.

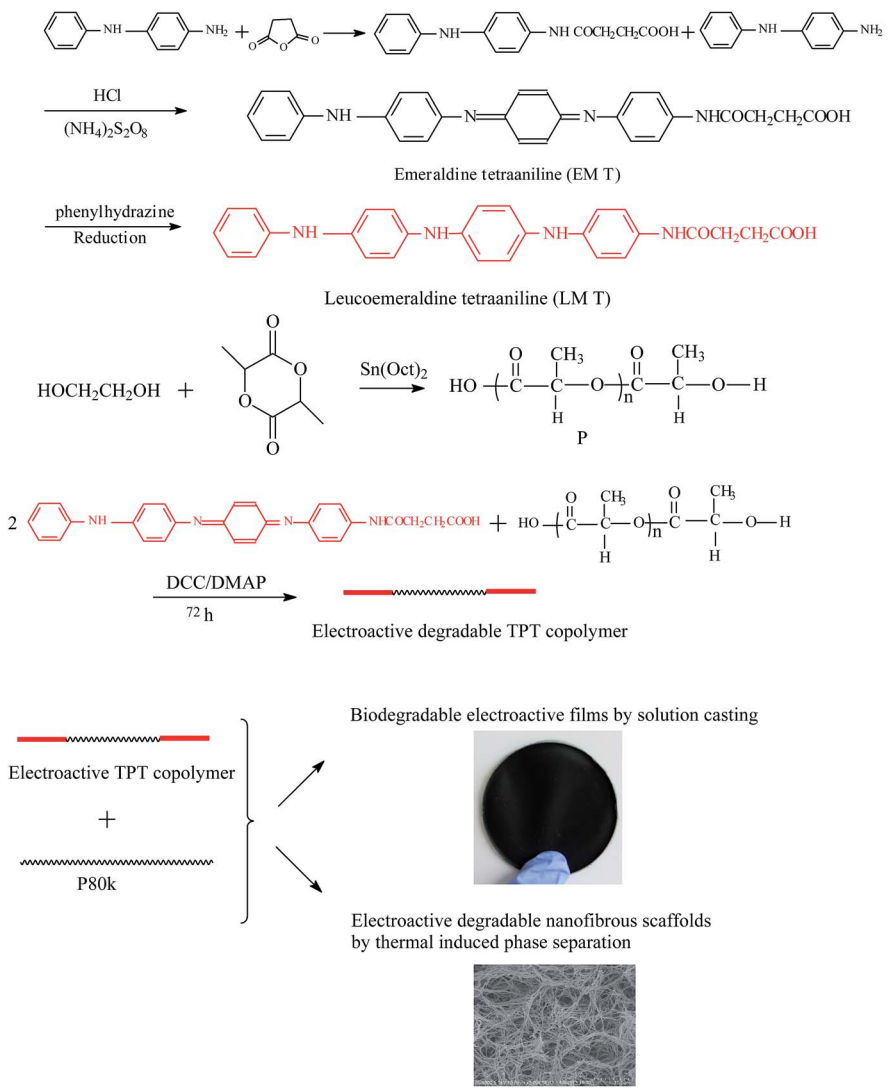

Scheme 1 Synthesis route of TPT and fabrication of electroactive biodegradable films and electroactive nanofibrous scaffolds.

Table 1 Composition of the used polymer blends (films and scaffolds). P80k: polylactide with a molecular weight of 80k; TPT: tetraaniline–polylactide1500–tetraaniline copolymer; P/TPT2: blends containing 2 wt% of tetraaniline; C: camphorsulfonic acid

Sample name	P80k (mg)	TPT (mg)	C (mg)
P80k	1000	0	0
P80k/TPT2	948	52	0
P80k/TPT5.5	858	142	0
P80k/TPT9	768	232	0
P80k/TPT2C	948	52	2.3
P80k/TPT5.5C	858	142	6.4
P80k/TPT9C	768	232	10.4

Characterization

The FT-IR spectra of the P1.5k, P80k and TPT block copolymer were recorded on a Nicolet 6700 FT-IR spectrometer (Thermo Scientific Instrument) in the 4000–600 cm^{-1} range.

The ^1H NMR (400 MHz) spectrum of the polymer was obtained using a Bruker Ascend 400 MHz NMR instrument, with $CDCl_3$ and DMSO-d_6 being used as the solvents for the polylactide and TPT copolymer and internal standards, respectively.

Gel permeation chromatography (GPC) was used to determine the molecular weights (M_n) of the polymers. The experiments were conducted on a Waters 1525 pump, a column heater equipped with two Waters Styragel columns (HT2 and HT4) and a Waters 2414 refractive index detector. THF was chosen as the mobile phase at a flow rate of 1 mL min^{-1}. The standard curve of molecular weight was calibrated by narrow polystyrene standards.

The UV-vis spectra of T and TPT in DMSO solution were recorded on a UV-vis spectrophotometer (PerkinElmer Lambda 35).

The thermal stability of the copolymers was tested by thermogravimetric analysis (TGA) using a Mettler-toledo TGA/DSC 1 thermogravimetric analyzer under a nitrogen atmosphere (nitrogen flow rate 50 mL min^{-1}) and a heating rate of 10 °C min^{-1}. The scan range was between 50 and 800 °C.

The glass transition temperature (T_g), melting temperature (T_m) and crystallinity (X_c) of the polymers were investigated using a TA Q200 DSC with a nitrogen flow rate of 50 mL min^{-1}. The samples were first heated to 200 °C, and the thermal history of polymers was removed by a 2 min equilibrium at 200 °C. Measurement was conducted by cooling the sample from 200 to −20 °C and the heating scan from −20 to 200 °C at a heating rate of 10 °C min^{-1}. T_g, T_m and X_c were obtained from the second heating scan. The crystallinity (X_c) was calculated by: $X_c = \Delta H_f/\Delta H_f^0 \times 100\%$, where ΔH_f is the enthalpy of fusion of polylactide crystallized in the blend, and ΔH_f^0 is the enthalpy of fusion of a 100% crystallized polylactide which is 93.6 J g^{-1} as reported in the previous work.[36]

Cyclic voltammetry (CV) of T and TPT was carried out on an Electrochemical Workstation (CHI 660D) interfaced and monitored with a PC computer. A three-electrode system, *i.e.* a platinum disc as the working electrode, a platinum-wire as the auxiliary electrode, and an Ag/AgCl as the reference electrode, was employed. The scan rate was 10 mV s^{-1}.

The mechanical properties of the blend films were determined on a MTS Criterion 43 instrument. Five or more rectangular specimens (80 × 5 mm^2) of each film were prepared and the thicknesses of the samples were measured using a thickness meter (Mitutoyo). The mechanical properties of the films were carried out according to the ASTM D 638M-89 standard with a load cell of 50 N, a speed of 2 mm min^{-1} and a gauge length of 30 mm.

Three circular specimens of each sample were immersed in deionized water. The change in the sample weight with time was periodically measured and the percentage weight gain of the water was calculated by the following equation: water adsorption% = $(W_t - W_o)/W_o \times 100\%$, where W_t and W_o are the weights of the equilibrated water swollen film and the dry film, respectively.

The morphology of the scaffolds was observed by using a field emission scanning electron microscope (FE-SEM, SU-8000, Hitachi, Japan). The average fiber diameter was tested using SEM images, where at least 100 measurements of fibers were selected throughout the matrix. Their average values and standard deviation were reported.

C2C12 cell adhesion and proliferation on the materials

The P80k/TPT films were cut into circular shapes that fit into 96-well plates and sterilized with ethylene oxide. After being washed three times with DPBS and twice with cell culture medium for 30 min each at 37 °C, the films were placed into a 96-well plate (Costar) and fixed with sterilized silicone rubber.

The C2C12 cell line was originally obtained from the ATCC (American Type Culture Collection) and incubated at 37 °C in a humidified incubator containing 5% CO_2. The complete growth medium was Dulbecco's Modified Eagle Medium (DMEM, GIBCO) supplemented with 10% fetal bovine serum (GIBCO), 1.0×10^5 U L^{-1} penicillin (Hyclone) and 100 mg L^{-1} streptomycin (Hyclone). 100 μL of the cell suspension containing approximately 3000 C2C12 cells was added into each well of the 96-well plate with P80k/TPT films. 10 μL of the AlamarBlue® (Invitrogen) reagent was added into each well after the cells being incubated for 24 h. The cells were cultured for another 6 h at 37 °C in a humidified incubator containing 5% CO_2 protected from direct light. 80 μL of the medium of each well was removed into a 96-well black plate (Costar). Fluorescence was read by a microplate reader (Molecular Devices). The cells were incubated for 1, 3 and 5 days and tested respectively. Cells seeded on P80k films served as the positive control group. Tests were repeated six times for each group.

100 μL of 5 wt% P80k/TPT in THF was coated onto an 18 mm × 18 mm cover slide and the solvent was removed by drying in air for 2 days. The cover slides placed in a 6-well plate (Costar) were sterilized with ethylene oxide for 5 h, and then washed three times with DPBS and twice with cell culture medium for 30 min each at 37 °C. The C2C12 cells were seeded on the cover slides at a density of approximately 1.0×10^5 cells per well. The plates were incubated for 48 h at 37 °C in a humidified incubator containing 5% CO_2. For cell morphology observation, the cover slides were fixed with 2.5% glutaraldehyde in DPBS at room temperature for 30 min and then washed with DPBS. The cells were stained by DPBS solution with fluorescein isothiocyanate (FITC) labeled phalloidin (Sigma) at a concentration of 5 μg mL^{-1} for 30 min at room temperature and then washed by deionized water three times. The cells were redyed with deionized water solution with DAPI (Sigma) at a concentration of 0.1 μg μL^{-1} for 5 min. For the cell viability test, the cover slides were washed three times with DPBS and stained with LIVE/DEAD® Viability/Cytotoxicity Kit (Molecular Probes) for 30 min at room temperature. Cell adhesion and morphology were observed under an inverted fluorescence microscope (IX53, Olympus).

Protein adsorption of the electroactive materials

The P80k, P80k/TPT2, P80k/TPT5.5, and P80k/TPT9 films were cut into circular shapes that fit into 24-well plates and washed three times with DPBS for 30 min each at 37 °C. The films were then placed into a 24-well plate (Costar). 1 mL DPBS containing 2.5% fetal bovine serum was added into each well. The plate was incubated at 37 °C for 20 h. Pierce™ BCA Protein Assay Kit (Thermo scientific) was used to quantify the concentration of the protein according to the manufacturer's instructions. The amount of proteins adsorbed to the films was determined by subtracting the amount of proteins left in the solution after adsorption from the amount of proteins in control solution (without films) under the same incubation conditions.

Effect of electrical stimulation on morphology and proliferation of C2C12 myoblasts

After sterilization with ethylene oxide, the P80k/TPT materials were put into a 24-well plate and washed three times by DPBS and twice by cell culture medium 30 min each at 37 °C. C2C12 cells were seeded on the substrates at a density of 5000 cells per well, and incubated for 24 h for adhesion. The electrical stimulation was then carried out by using the function/arbitrary waveform generator (Rigol DS1022) to generate the electrical signals, and the oscilloscope (Rigol DS1074) to check the

signals. The electrical signal, which was a square wave with the frequency of 50 Hz, 50% duty cycle and electrical potential of 0.2 V, was transmitted to the P80k/TPT through platinum electrodes for 1 h every day. To prevent from ionization damage, the media were changed immediately after the electrical stimulation. The electrical stimulation was carried out for 5 days and the cell viability was quantified with the AlamarBlue assay as described on day 1, 3 and 5, respectively. Cells on P80k/TPT substrates without electrical stimulation served as the positive groups. Tests were repeated six times for each group.

The cells on P80k/TPT substrates were washed and stained with a LIVE/DEAD® Viability/Cytotoxicity Kit for 30 min at room temperature after 5 days of electrical stimulation. The fluorescent images were observed under an inverted fluorescence microscope (Olympus, IX53).

Statistical analysis

All the data were expressed as mean ± standard deviation. The data were statistically analyzed by a one-way ANOVA test followed by using the S–N–K test method. Data were analyzed using the SPSS18.0 statistical package. Differences were considered statistically significant when $p < 0.05$.

Results and discussion

Synthesis of P and TPT copolymers

Polylactide has good biocompatibility, biodegradability and mechanical strength. It is widely used in tissue engineering applications.[37,38] However, polylactide does not have bioactivity to tune the cellular activity during tissue repair.[39,40] We synthesized a new block copolymer TPT in this work by introducing T to P to endow the TPT copolymer electroactivity which could be used to tune the cellular behavior. However, TPT has poor mechanical properties due to its low molecular weight. We therefore blend TPT with P80k to obtain electroactive degradable blends with good mechanical strength. We then further fabricated these copolymer blends into electroactive nanofibrous scaffolds which are intended for tissue engineering applications where electroactivity is needed. The P block could improve the miscibility of TPT and P80k. By changing the weight ratio of TPT and P80k, it is easy to control the T content in the blends accurately in this way.

The FT-IR spectra of P1.5k, T, TPT and P80k/TPT9 are shown in Fig. S1 in the ESI.† The peaks at 1755 cm^{-1} and 1084 cm^{-1} in curve a of P1.5k correspond to ester groups (–COO–) and ether groups (–C–O–C–) in polylactide. In curve b, the absorption peaks at 1609 cm^{-1} and 1525 cm^{-1} are characteristic of the stretching vibration bands of quinoid rings and benzenoid rings, respectively. The bands at 1713 cm^{-1} and 1657 cm^{-1} are assigned to the absorptions from the carbonyl group (–CO–) in –COOH and the amide group (–NHCO–) in T. Compared to curves a and b, the TPT copolymer showed bands at 1756 cm^{-1} and 1088 cm^{-1} from the P segment, and bands at 1599 cm^{-1} and 1505 cm^{-1} are assigned to quinoid rings and benzenoid rings from the T segment, indicating that the TPT copolymer was obtained. The ester peak shifted to a lower peak at 1748 cm^{-1} compared to that in TPT, indicating that the hydrogen bonds are formed between the ester group of P80k and the –NH– group in TPT.

The NMR spectrum was also used to confirm the chemical structure of the polymers. The ^1H NMR spectrum of P1.5k is

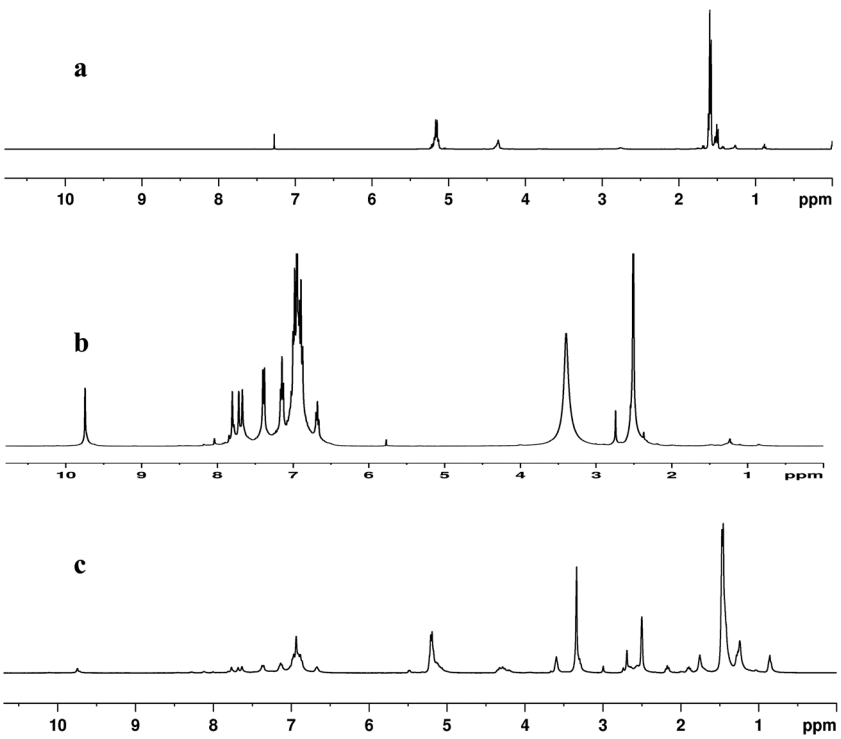

Fig. 1 ^1H-NMR spectra of (a) P1.5k, (b) T and (c) the TPT copolymer.

Table 2 Molecular weight of polylactide and TPT block copolymer

Sample	M_n from ^{1}H NMR	M_n from GPC	MWD
P1.5k	1500	2900	1.1
P80k	79 000	10 900	1.3
TPT	2450	3900	1.1

shown in Fig. 1(a). The molecular weight of P was determined by comparing the peak integral of –CH– protons ($\delta = 5.2$ ppm) with the sum of –CH– protons next to the terminal hydroxyl groups ($\delta = 4.4$ ppm) and the $-CH_2-$ protons in ethylene glycol. The molecular weights calculated by NMR for the low molecular weight P and high molecular weight P are 1500 and 79 000, respectively, which were very close to theoretical molecular weights, and agreed well with the GPC results as shown in Table 2. This indicated the successful synthesis of the polylactide.

The ^{1}H NMR spectrum of TPT is shown in Fig. 1(c). TPT: ^{1}H NMR (400 MHz, DMSO-d_6): $\delta = 9.74$ (s, 1H, –NHCO–), $\delta = 7.77$ (s, 1H, Ar-H), $\delta = 7.69$ (s, 1H, –NH–), $\delta = 7.64$ (s, 1H, –NH–), $\delta = 7.36$–7.38 (d, 2H, Ar-H), $\delta = 7.13$–7.15 (d, 2H, Ar-H), $\delta = 6.98$–6.88 (m, 12H, Ar-H), $\delta = 6.68$–6.65 (d, 2H, Ar-H), $\delta = 2.73$–2.68 (t, 4H, $-CH_2CH_2-$) for the T segment, and $\delta = 5.19$ (t, 2H, poly –CH–), $\delta = 4.32$–4.27 (m, 4H, –CH– end and –CH– from ethylene glycol), $\delta = 1.46$–1.48 (m, 3H, poly $-CH_3$), $\delta = 1.25$ (d, 3H, $-CH_3$ end) for the polylactide segment. The peak of $-CH_2CH_2-$ from T changed to a lower chemical shift in the TPT copolymer because of the coupling reaction between the hydroxyl groups at the polylactide chain end and the carboxyl groups of T. The ratio of the integrals of the $-CH_2CH_2-$ group at 2.73–2.68 ppm and the –CH– group at 5.19 ppm from P1.5k in the TPT copolymers was about 1 : 3. All these data confirm the successful esterification between the T and P1.5k. The molecular weight of TPT determined from GPC was about 1000 higher than that of P1.5k, as shown in Table 2. This also indicated that the TPT triblock copolymer was obtained.

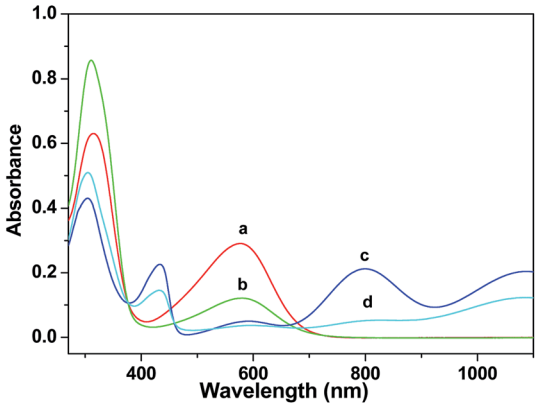

Fig. 2 UV-vis spectra of (a) T, (b) TPT, (c) C doped T and (d) C doped TPT.

Electroactivity of the copolymers

Fig. 2 shows the UV-vis spectra of T, the TPT copolymer and their doped forms as curves a, b, c and d, respectively. The UV spectra of both T and TPT showed two characteristic peaks at 318 nm and 580 nm, which are attributed to the π–π^* transition of the benzene ring and the benzenoid to quinoid excitonic transition, respectively. When T and the TPT copolymer were doped with C in DMSO, the peak at 580 nm almost disappeared, and a new absorption peak appeared at 432 nm along with a slight blue shift of the benzenoid absorption peak to 309 nm owing to the formation of delocalized polarons.[41] The peak at 798 nm corresponding to the localization of the radical polaron confirms the generation of emeraldine salts.[42,43]

The cyclic voltammograms of T and the TPT copolymer are shown in Fig. 3. The TPT copolymer and T were dissolved in DMSO and doped by C solution. The cyclic voltammograms of T in Fig. 3(a) and its copolymer in Fig. 3(b) showed two pairs of well-defined reduction/oxidation peaks (0.34 V and 0.54 V), which are attributed to the redox process from the "leucoemeraldine" to the "emeraldine" form, and then from the "emeraldine" to the "pernigraniline" state. The redox peaks of the copolymer are the same as those of monomer T, indicating that the polylactide chains have no effect on the reduction/oxidation of the T segments. All these UV-visible and CV results confirmed the good electroactivity of the TPT copolymer.

Thermal properties of the copolymer blends

The thermal property of the copolymer blends was studied by TGA and DSC. TGA is used to determine the thermal stability of the blends, and the results are plotted in Fig. 4. When the

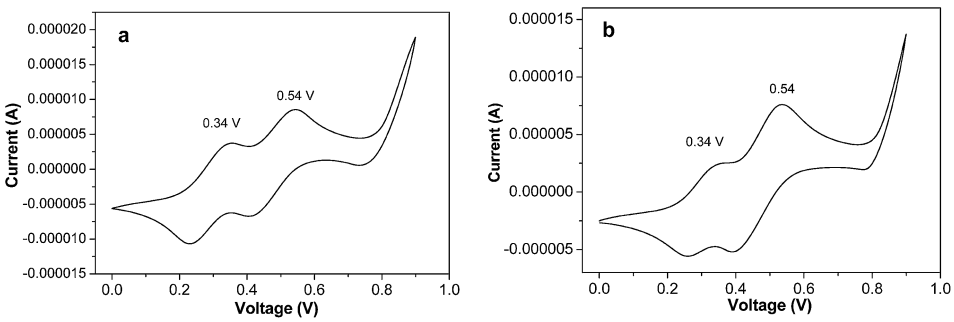

Fig. 3 Cyclic voltammograms of (a) T and (b) the TPT copolymer.

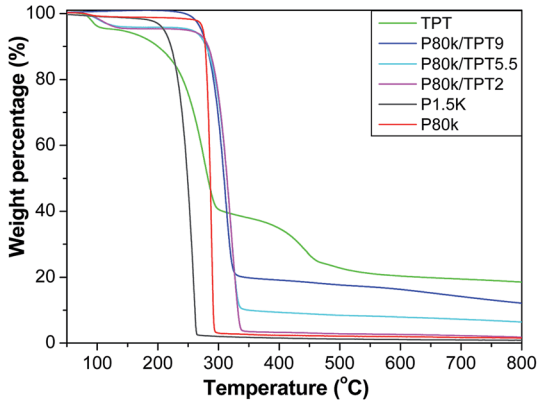

Fig. 4 TGA curves of the polymers.

temperature was increased from 100 to 200 °C, a slight weight loss from P, TPT and their blends was observed. This is ascribed to moisture and to the loss of other solvents trapped in the polymer. In the case of pure P1.5k, a major weight loss between 200 °C and 265 °C occurred, and the weight loss above 265 °C was almost 100%, indicating the degradation of the P main chain. The P80k showed a similar degradation behavior to that of P1.5k. However, the P main chain degraded at a higher temperature between 270 and 295 °C, indicating a better thermal stability due to the stronger macromolecular entanglement between the P chains. In the case of TPT, it showed a two stage degradation behavior. The first evident weight loss occurred between 200 °C and 300 °C, and was assigned to the degradation of the less thermally stable P segments in the copolymer. The second obvious weight loss took place between 300 and 470 °C, and was attributed to the degradation of the T segment. The higher thermal stability of the TPT copolymer compared to the pure P1.5k was caused by the better thermal stability of T segments. The second degradation stage was used to calculate the T content in the TPT copolymer since the P segment was almost completely degraded.[41] The content of T in the copolymer was about 38 wt% determined by the second degradation stage which was in accordance with the feed ratio of the copolymer. The thermal stability of the blend materials was intermediate between that of P80k and TPT copolymer. The thermal stability increased with increasing TPT copolymer content in the blends, owing to the better thermal stability of the TPT copolymer.

The T_g and T_m of the copolymer blends were tested by DSC, and the results are listed in Table 3. The T_g of TPT was about 36.1 °C, which is higher than that of P1.5k which is about 25.5 °C, because the rigid T segment hindered the movement of the middle P segment. The T_m of the TPT polymer is not detected, indicating that the TPT copolymer is in an amorphous state. This could be because that the end rigid T segments in the TPT copolymer seriously disturbed the crystallization of the P segments.

The T_g and T_m of P80k were 65.1 °C and 175.3 °C, respectively. The P80k/TPT2, P80k/TPT5.5 and P80k/TPT9 blends showed a lower T_g and T_m than P80k, because the addition of TPT to the P80k weakened the interactions and increased the mobility of the P segment. As a consequence, the P segment can move at lower temperature in the blends compared to that of pure P80k. The T_g of the copolymer blends also increased accordingly with respect to the decrease of the TPT content in the blends, because the higher content of TPT in the blend has a stronger plasticizing effect.

The crystallinity (X_c) of the copolymer blends was lower than that of pure P80k and decreased in order with increasing the TPT content in the blends. This is also because the TPT molecule disturbed the crystallization process of the P segment. It is important to point out that although the X_c of the blends decreased compared to the pristine P80k. However, the X_c values just decreased slightly. This provides the possibility of using TIPS to fabricate the nanofibrous scaffolds from the polymer blends, as a certain degree of crystallinity of the polymer is required for TIPS to prepare nanofibrous scaffolds.[44]

Water absorption of the blend films

Water uptake of the films with different TPT contents was determined and the results are displayed in Table 4. The water absorption of P80k is 2.1%, indicating a very hydrophobic material. The water uptake of P80k/TPT blends increased from 3.1% to 13.1%, indicating that the hydrophilicity of the blend films increased with increasing TPT content in the blends. Moreover, the water absorption of the doped P80k/TPT blend films in the range of 4.4% and 15.0% is higher than those of the undoped films, because the formation of emeraldine salt further increased the hydrophilicity of the materials. The doped P80k/TPT film showed much higher water absorption than P80k. This may overcome the hydrophobicity of the polylactide, and probably leading to a better cell adhesion of the blend films.

Table 3 T_g and T_m of the polymers determined by DSC[a]

Sample code	T_g (°C)	T_m (°C)	X_c
TPT	36.1 ± 3.8	*	*
P80k	65.1 ± 3.8	175.3 ± 0.1	53.4 ± 6.3
P80k/TPT2	59.6 ± 0.1	175.1 ± 0.4	39.4 ± 2.4
P80k/TPT5.5	58.6 ± 0.4	174.5 ± 0.3	38.1 ± 1.4
P80k/TPT9	57.2 ± 0.7	173.8 ± 0.9	33.7 ± 4.0

[a] *: not detected.

Table 4 Water absorption of the blend films

Sample name	Water absorption (%)
P80k	2.1 ± 0.6
P80k/TPT2	3.1 ± 1.0
P80k/TPT5.5	5.2 ± 0.9
P80k/TPT9	13.1 ± 0.6
P80k/TPT2C	4.4 ± 0.2
P80k/TPT5.5C	10.4 ± 1.9
P80k/TPT9C	15.0 ± 0.7

Table 5 Mechanical properties of the blend films

Sample name	Stress at break (MPa)	Strain at break (%)	*E*-modulus (MPa)
P80k	20.5 ± 0.5	11.9 ± 0.3	814.7 ± 11.9
P80k/TPT2	18.6 ± 0.8	7.4 ± 1.1	796.4 ± 68.5
P80k/TPT5.5	17.0 ± 1.2	5.5 ± 0.7	785.9 ± 34.1
P80k/TPT9	14.9 ± 0.6	4.5 ± 0.4	741.1 ± 45.1
P80k/TPT2C	19.1 ± 0.8	19.1 ± 1.2	708.5 ± 52.0
P80k/TPT5.5C	16.5 ± 0.3	14.6 ± 2.0	602.9 ± 15.2
P80k/TPT9C	12.7 ± 0.7	13.0 ± 0.8	482.6 ± 33.4

Mechanical properties of the films

Mechanical properties of biomaterials are quite important for their use in tissue engineering, since the biomaterials need to withstand the mechanical stress during neogenesis. The mechanical strength of copolymer blend films was determined by a tensile test, and the results are displayed in Table 5. The stress at break and *E*-modulus of pure P80k were 20.5 MPa and 814.7 MPa, respectively. The stress at break of the undoped and doped P80k/TPT blend film was lower compared to that of P80k, and they are between 19.1 MPa and 12.7 MPa. The *E*-modulus of the doped and undoped blend copolymer showed a similar trend to that of stress at break, and they decreased accordingly with increasing the TPT content in the blends, because the TPT molecules disrupted the ordered structure of P and weakened the inter- and intra-molecular interaction between the P macromolecules. The *E*-modulus of the C doped P80k/TPT blend is lower than that of the undoped counterparts, probably because of the plasticizing effect of the dopants in the matrix. The modulus of the blend films is much higher than that of the electroactive poly(ester-amide)-*graft*-tetraaniline copolymer which is 20 ± 2.5 MP.[45] It should be noted that although the *E*-modulus of the blend films was decreased, a moderate *E*-modulus of the materials remained.

One disadvantage of using P as a biomaterial is its brittleness.[46,47] The strain at break of the P80k in this study is 11.9%. The P80k/TPT blend film showed a lower strain at break between 7.4% and 4.5%. However, the C doped P80k/TPT blend showed a much higher strain at break in the range of 19.1% and 13.0%, compared to that of pure P80k. This overcomes the brittleness of P and endowed the C doped blend materials a better handling ability during the tissue engineering applications.[48]

Morphology of electroactive nanofibrous scaffolds

TIPS is a robust and powerful technique to create nanofibrous structures of the scaffolds. However, most of the synthetic materials used to create nanofibrous scaffolds are polylactide and poly(lactide-*co*-glycolide) copolymers. These aliphatic polyesters have good biocompatibility and biodegradability. However, they lack of bioactivity.[49] It remains a challenge to create functional nanofibrous scaffolds by TIPS. We blended the electroactive degradable TPT copolymer with P80k, and demonstrated the good electroactivity and mechanical properties of the blends. We further fabricated these electroactive degradable blends into electroactive nanofibrous scaffolds by TIPS. The nanofibrous structures of the P80k, P80k/TPT2, P80k/TPT5.5 and P80k/TPT9 are shown in Fig. 5. We can see that all the systems formed porous scaffolds with a fiber diameter between 100 nm and 500 nm, which could mimic the structure of the natural ECM. The diameters of the scaffolds of P80k, P80k/TPT2, P80k/TPT5.5 and P80k/TPT9 are 195 ± 36, 207 ± 31, 224 ± 33 and 268 ± 37 nm, respectively, which increased with increasing the TPT content in the blends.

We also studied the effect of polymer concentration and phase separation temperature on the diameter of the nanofibers. The SEM images of P80k/TPT with different polymer concentrations and phase separation temperatures are shown in Fig. S2.† The diameter of the 5 wt% P80k/TPT9 with a phase separation temperature at −20 °C and at −80 °C was 268 ± 37 and 284 ± 58 nm, respectively. In the case of the 7.5 wt% P80k/TPT9 with a phase separation temperature at −20 °C and at −80 °C, the diameter of the fibers slightly increased from 224 ± 33 to 275 ± 47 nm. For samples with the same phase separation temperature, the diameter of the nanofibers with 5 wt% of the polymer solution was bigger than that with 7.5 wt% as shown in Table 6. By comparing the images of Fig. S2a with S2c, and Fig. S2b with d in the ESI,† we found that the scaffolds of a and b showed a more porous structure than c and d, due to the lower polymer concentration. We could thus tune the diameter of the nanofibers and pore size of the scaffolds by controlling the polymer concentration and phase separation temperature.

Cell adhesion and proliferation assay of C2C12 myoblasts

P has good biocompatibility and is widely used in tissue engineering.[50,51] In our work, the P80k film was used as the control group to evaluate the biocompatibility of the P80k/TPT blend polymers. C2C12 myoblasts have been proved sensitive to electrical stimulations and this makes C2C12 myoblasts an ideal cell type to evaluate the biocompatibility of electroactive

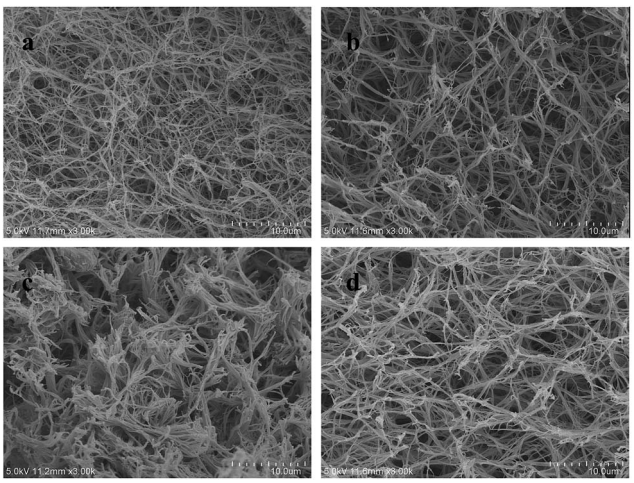

Fig. 5 SEM images of (a) P80k, (b) P80k/TPT2, (c) P80k/TPT5.5 and (d) P80k/TPT9, the concentration of the blend was 5 wt% and the phase separation temperature was −20 °C for all the samples.

Table 6 The diameter of the nanofibers of the scaffolds

Sample code	Polymer concentration (wt%)	Phase separation temperature (°C)	Fiber diameter (nm)
P80k	5	−20	195 ± 36
P80k/TPT2	5	−20	207 ± 31
P80k/TPT5.5	5	−20	224 ± 33
P80k/TPT9	5	−20	268 ± 37
P80k/TPT9	5	−80	284 ± 58
P80k/TPT9	7.5	−20	224 ± 44
P80k/TPT9	7.5	−80	275 ± 47

materials.[52,53] After C2C12 cells being incubated on the P80k/TPT substrates for 48 h, the cells were stained by a LIVE/DEAD® Viability/Cytotoxicity Kit and the results are shown in Fig. 6. Dominant live cells (green) were observed for all the groups, and dead cells (red) were barely found. There was no significant difference between P80k/TPT and P80k groups. These illustrated that the P80k/TPT blends are not toxic.

Cytoskeleton staining is a good way to detect the change of cell morphology which is influenced by the culture substrate. C2C12 cells on P80k/TPT substrates were stained by FITC labeled phalloidin and DAPI after being incubated for 48 h (Fig. 6). C2C12 myoblast cells for all the groups showed a normal spindle-like morphology, and there was no significant difference between P80k/TPT groups and the P80k group. Furthermore, the C2C12 cell proliferation on P80k/TPT2 and P80k/TPT5.5 is much better than that on P80k. These results indicated that the P80k/TPT films are nontoxic and ideal substrates for C2C12 cells to adhere.

Cell proliferation of C2C12 myoblasts on the P80k/TPT blend films was evaluated by the AlamarBlue® assay and the results are shown in Fig. 7. The cell number on all the groups showed a continuous increase from day 1 to day 5, indicating that all the P80k/TPT groups supported the proliferation of C2C12 cells. The cell viability of C2C12 cells on P80k/TPT2 and P80k/TPT5.5

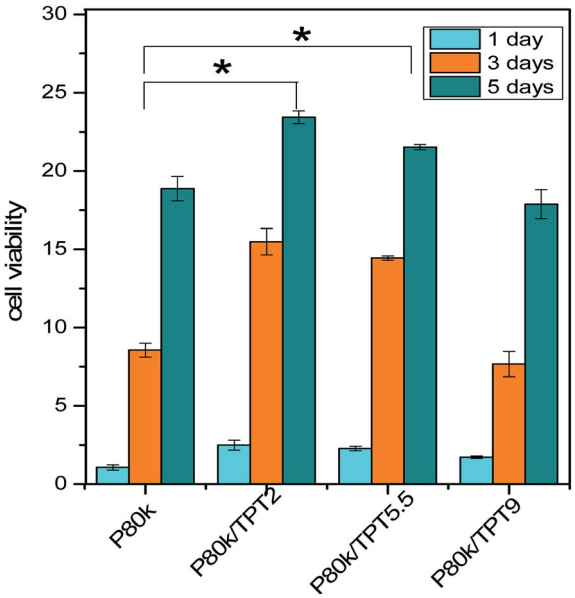

Fig. 7 Cell viability of C2C12 cells on P80k/TPT films with P80k served as the control group. The cell viability of C2C12 on P80k/TPT2 and P80k/TPT5.5 films was higher than that on the P80k film. * indicates statistically significant differences between the groups (*$p < 0.05$).

films was higher than that on P80k films ($p < 0.05$). There was no significant difference between the cell viability of C2C12 cells on P80k/TPT9 films and P80k films ($p > 0.05$). The results demonstrated that these electroactive P80k/TPT blend materials with a suitable content of the AT segments are non-toxic and that they enhanced the proliferation of C2C12 myoblasts without electrical stimulation. These results indicated that these electroactive degradable materials would work better as tissue engineering scaffolds compared to polylactide.

To further explore the possible mechanism for the enhanced C2C12 cell proliferation on the electroactive materials, the protein adsorption tests on these electroactive materials were

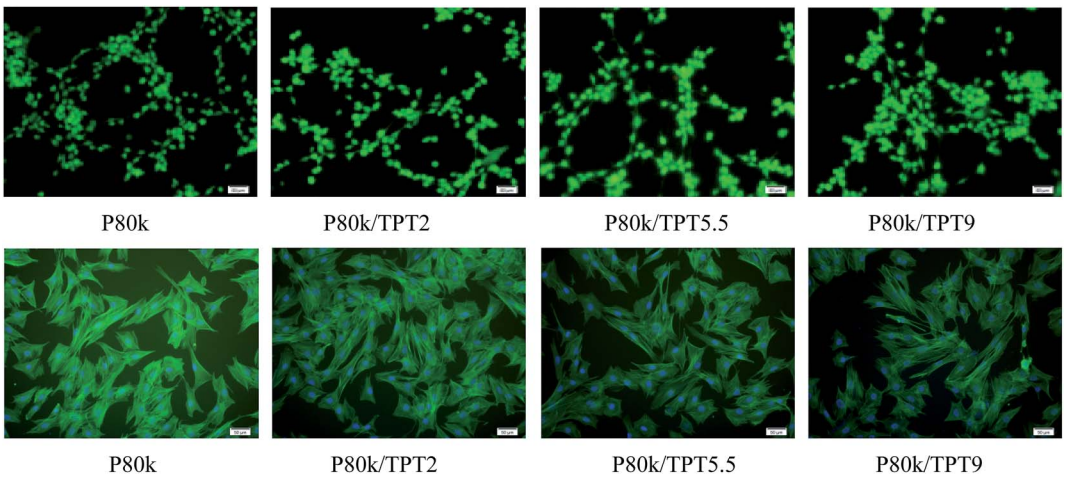

Fig. 6 Fluorescent images of C2C12 cells on P80k/TPT substrates stained by LIVE/DEAD® Viability/Cytotoxicity Kit (top) and stained by FITC labeled phalloidin and DAPI (bottom) after being cultured for 48 h. Scale bars represent 50 μm.

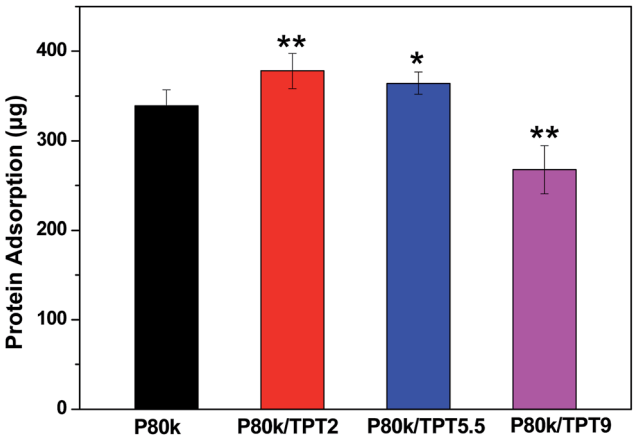

Fig. 8 Protein adsorption of P80k, P80k/TPT2, P80k/TPT5.5, and P80k/TPT9 substrates incubated for 20 h in fetal bovine serum, *p < 0.10 and **p < 0.05.

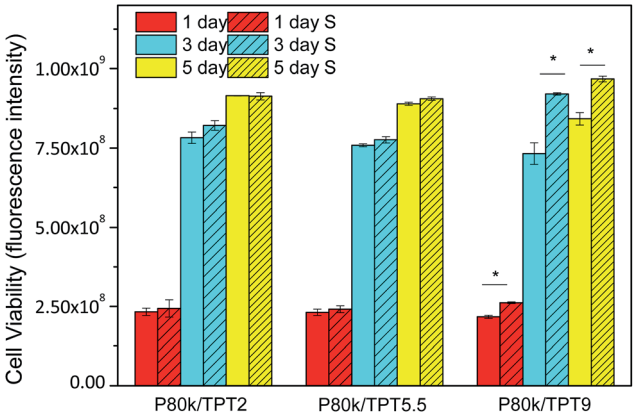

Fig. 9 Cell viability of C2C12 cells on P80k/TPT2, P80k/TPT5.5 and P80k/TPT9 substrates stimulated by the electrical signal for 1, 3, and 5 days (*p < 0.05, S: stimulated by the electrical signal).

carried out, since proteins adsorbed onto a biomaterial surface usually served as a mediating layer for cellular activities after the implantation of the biomaterials. The protein adsorption amount on P80k/TPT2 and P80k/TPT5.5 substrates was much higher than that on the P80k film as shown in Fig. 8, and these results are in accordance with the C2C12 cell adhesion and proliferation results in Fig. 7. This was because the electroactive material adsorbed more ECM proteins on its surface,[54] and these ECM proteins could enhance the cell adhesion and proliferation for biomaterials.

Influence on proliferation and morphology of C2C12 cells stimulated by electrical signal

To evaluate the influence of electrical stimulation on C2C12 myoblast morphology and proliferation on these electroactive materials, the C2C12 myoblasts were seeded on the P80k/TPT substrates and stimulated by the electrical signal for 1, 3 and 5 days. The cell viability was evaluated by the AlamarBlue® assay and the results are shown in Fig. 9 and Fig. S3.† The cell proliferation of C2C12 myoblasts on P80k/TPT2, P80k/TPT2C, P80k/TPT5.5, and P80k/TPT5.5C with electrical stimulation is higher than those of without electrical stimulation. However, there was no significant difference between the electrical stimulation group and the unstimulated group (p > 0.05). In the case of samples P80k/TPT9 and P80k/TPT9C, the cell viability showed a significant increase after the electrical stimulation compared to the unstimulated groups (p < 0.05), demonstrating that the electroactive P80k/TPT9 substrate could significantly promote the cell proliferation of C2C12 myoblasts by electrical stimulation. These cell proliferation results indicated that these electroactive materials could significantly enhance the C2C12 myoblast proliferation *via* electrical stimulation with appropriate amounts of the TPT content.

To visualize the cell morphology and cell viability, the C2C12 myoblasts cultured on P80k/TPT substrates were stained with a LIVE/DEAD® Viability/Cytotoxicity Kit after 5 days of electrical

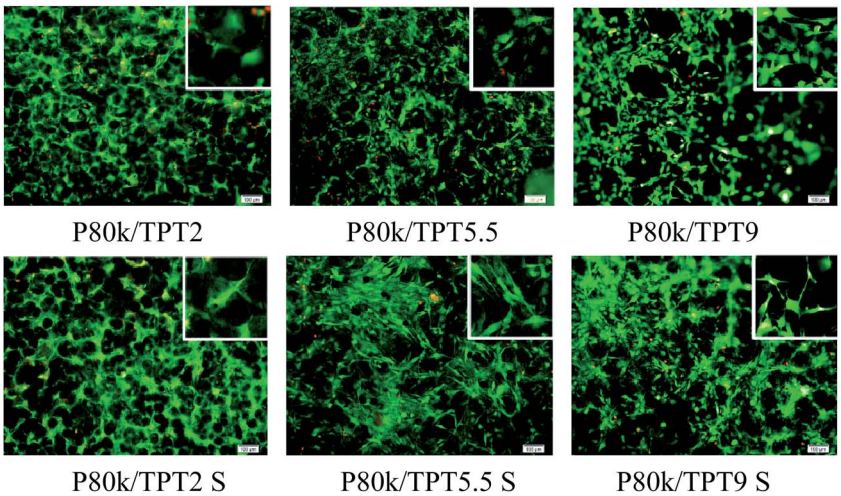

Fig. 10 Fluorescent images of C2C12 cells on P80k/TPT substrates stained by a LIVE/DEAD® Viability/Cytotoxicity Kit. Scale bars represent 100 μm. S: stimulated by the electrical signal.

stimulation. The fluorescent images of the C2C12 cell morphology are shown in Fig. 10 and 4S.† Dominant live cells (green) were observed in all the groups, and the C2C12 myoblasts on P80k/TPT9, P80k/TPT9C, and P80k/TPT5.5 tended to gather together and showed a more elongated morphology in the electrical stimulation groups compared to the unstimulated groups, probably because the electroactive substrates could accelerate the communication between the cells *via* electrical stimulation. All these results demonstrated that the electroactive materials with electrical stimulation have a positive effect on the desirable cell morphology change and cell proliferation of C2C12 myoblasts.

Conclusions

Electroactive biodegradable nanofibrous biomimetic scaffolds from the blends of polylactide and an electroactive degradable tetraaniline–polylactide–tetraaniline (TPT) copolymer *via* a thermally induced phase separation technique have been presented. The structure and electroactivity of the TPT copolymer were confirmed by FT-IR, NMR, UV and CV measurements. The thermal stability of the blends increased with increasing the TPT content. Water uptake of the blend polymers is much higher than that of the pure polylactide, indicating a more hydrophilic material. The *E*-modulus of the blend films decreased with increasing TPT content, and the strain of the doped blend film is much higher than that of polylactide. The nanofibrous scaffolds from the blends are fabricated by a thermally induced phase separation technique. The diameters of the fibers between 200 and 500 nm are controlled by the concentration of the polymer, phase separation temperature and TPT content in the blends. These electroactive degradable materials are nontoxic and enhance the adhesion and proliferation of the C2C12 myoblast cells compared to polylactide, probably because of the more proteins adsorbed on the electroactive materials than that of polylactide. The electroactive materials significantly improved the cell proliferation of C2C12 myoblasts under electrical stimulation. This work offers new ways to create functional nanofibrous scaffolds for tissue engineering applications.

Acknowledgements

The authors gratefully acknowledge the Natural Science Foundation of China (grant number: 21304073) and "the Fundamental Research Funds for the Central Universities" (Grant no. xjj2013029), and the Scientific Research Foundation for the Returned Overseas Chinese Scholars for financial support of this work.

References

1 L. S. Nair and C. T. Laurencin, *Prog. Polym. Sci.*, 2007, **32**, 762–798.
2 E. S. Place, J. H. George, C. K. Williams and M. M. Stevens, *Chem. Soc. Rev.*, 2009, **38**, 1139–1151.
3 W. J. Li, R. Tuli, C. Okafor, A. Derfoul, K. G. Danielson, D. J. Hall and R. S. Tuan, *Biomaterials*, 2005, **26**, 599–609.
4 H. J. Lee, S. H. Ahn and G. H. Kim, *Chem. Mater.*, 2012, **24**, 881–891.
5 N. E. Zander, J. A. Orlicki, A. M. Rawlett and T. P. Beebe, *ACS Appl. Mater. Interfaces*, 2012, **4**, 2074–2081.
6 B. L. Guo and P. X. Ma, *Sci. China: Chem.*, 2014, **57**, 490–500.
7 H. Shin, S. Jo and A. G. Mikos, *Biomaterials*, 2003, **24**, 4353–4364.
8 Z. W. Ma, M. Kotaki, R. Inai and S. Ramakrishna, *Tissue Eng.*, 2005, **11**, 101–109.
9 Y. X. Liu, S. Rayatpisheh, S. Y. Chew and M. B. Chan-Park, *ACS Appl. Mater. Interfaces*, 2012, **4**, 1378–1387.
10 H. S. Koh, T. Yong, C. K. Chan and S. Ramakrishna, *Biomaterials*, 2008, **29**, 3574–3582.
11 T. G. Kim, H. Shin and D. W. Lim, *Adv. Funct. Mater.*, 2012, **22**, 2446–2468.
12 A. Mujeeb, A. F. Miller, A. Saiani and J. E. Gough, *Acta Biomater.*, 2013, **9**, 4609–4617.
13 S. Jana, A. Cooper, F. Ohuchi and M. Q. Zhang, *ACS Appl. Mater. Interfaces*, 2012, **4**, 4817–4824.
14 X. J. Ma, J. Ge, Y. Li, B. L. Guo and P. X. Ma, *RSC Adv.*, 2014, **4**, 13652–13661.
15 J. M. Holzwarth and P. X. Ma, *J. Mater. Chem.*, 2011, **21**, 10243–10251.
16 Y. S. Nam and T. G. Park, *Biomaterials*, 1999, **20**, 1783–1790.
17 A. S. Rowlands, S. A. Lim, D. Martin and J. J. Cooper-White, *Biomaterials*, 2007, **28**, 2109–2121.
18 N. K. Guimard, N. Gomez and C. E. Schmidt, *Prog. Polym. Sci.*, 2007, **32**, 876–921.
19 B. L. Guo, A. Finne-Wistrand and A. C. Albertsson, *Prog. Polym. Sci.*, 2013, **38**, 1263–1286.
20 L. C. Li, J. Ge, B. L. Guo and P. X. Ma, *Polym. Chem.*, 2014, **5**, 2880–2890.
21 S. H. Bhang, S. I. Jeong, T. J. Lee, I. Jun, Y. B. Lee, B. S. Kim and H. Shin, *Macromol. Biosci.*, 2012, **12**, 402–411.
22 J. W. Xie, M. R. MacEwan, S. M. Willerth, X. R. Li, D. W. Moran, S. E. Sakiyama-Elbert and Y. N. Xia, *Adv. Funct. Mater.*, 2009, **19**, 2312–2318.
23 J. Y. Lee, C. A. Bashur, A. S. Goldstein and C. E. Schmidt, *Biomaterials*, 2009, **30**, 4325–4335.
24 J. Nam, Y. Huang, S. Agarwal and J. Lannutti, *Tissue Eng.*, 2007, **13**, 2249–2257.
25 M. Simonet, O. D. Schneider, P. Neuenschwander and W. J. Stark, *Polym. Eng. Sci.*, 2007, **47**, 2020–2026.
26 M. Simonet, N. Stingelin, J. G. F. Wismans, C. W. J. Oomens, A. Driessen-Mol and F. P. T. Baaijens, *J. Mater. Chem. B*, 2014, **2**, 305–313.
27 H. C. Zhao, B. Zhu, J. Sekine, S. C. Luo and H. H. Yu, *ACS Appl. Mater. Interfaces*, 2012, **4**, 680–686.
28 N. K. E. Guimard, J. L. Sessler and C. E. Schmidt, *Macromolecules*, 2009, **42**, 502–511.
29 B. L. Guo, A. Finne-Wistrand and A.-C. Albertsson, *Macromolecules*, 2010, **43**, 4472–4480.
30 B. L. Guo, A. Finne-Wistrand and A. C. Albertsson, *Chem. Mater.*, 2011, **23**, 4045–4055.

31 B. L. Guo, A. Finne-Wistrand and A. C. Albertsson, *Macromolecules*, 2011, **44**, 5227–5236.
32 B. L. Guo, A. Finne-Wistrand and A. C. Albertsson, *Biomacromolecules*, 2011, **12**, 2601–2609.
33 B. L. Guo, A. Finne-Wistrand and A. C. Albertsson, *J. Polym. Sci., Part A: Polym. Chem.*, 2011, **49**, 2097–2105.
34 B. L. Guo, A. Finne-Wistrand and A. C. Albertsson, *Biomacromolecules*, 2010, **11**, 855–863.
35 X. H. Liu and P. X. Ma, *Biomaterials*, 2010, **31**, 259–269.
36 O. Martin and L. Averous, *Polymer*, 2001, **42**, 6209–6219.
37 J. K. Oh, *Soft Matter*, 2011, **7**, 5096–5108.
38 A. Duda and S. Penczek, *Polimery*, 2003, **48**, 16–27.
39 B. L. Guo, A. Finne-Wistrand and A. C. Albertsson, *Macromolecules*, 2012, **45**, 652–659.
40 R. M. Rasal, A. V. Janorkar and D. E. Hirt, *Prog. Polym. Sci.*, 2010, **35**, 338–356.
41 B. L. Guo, A. Finne-Wistrand and A. C. Albertsson, *Chem. Mater.*, 2011, **23**, 1254–1262.
42 J. Gao, D. G. Liu, J. M. Sansiñena and H. L. Wang, *Adv. Funct. Mater.*, 2004, **14**, 537–543.
43 L. H. Huang, J. Hu, L. Lang, X. Wang, P. B. Zhang, X. B. Jing, X. H. Wang, X. S. Chen, P. I. Lelkes, A. G. MacDiarmid and Y. Wei, *Biomaterials*, 2007, **28**, 1741–1751.
44 K. M. Woo, V. J. Chen and P. X. Ma, *J. Biomed. Mater. Res., Part A*, 2003, **67A**, 531–537.
45 H. T. Cui, Y. D. Liu, M. X. Deng, X. Pang, P. B. A. Zhang, X. H. Wang, X. S. Chen and Y. Wei, *Biomacromolecules*, 2012, **13**, 2881–2889.
46 S. S. Ray, *Acc. Chem. Res.*, 2012, **45**, 1710–1720.
47 M. L. Robertson, J. M. Paxton and M. A. Hillmyer, *ACS Appl. Mater. Interfaces*, 2011, **3**, 3402–3410.
48 P. Plikk, S. Malberg and A. C. Albertsson, *Biomacromolecules*, 2009, **10**, 1259–1264.
49 Z. W. Ma, C. Y. Gao, Y. H. Gong and J. C. Shen, *Biomaterials*, 2005, **26**, 1253–1259.
50 F. P. W. Melchels, J. Feijen and D. W. Grijpma, *Biomaterials*, 2009, **30**, 3801–3809.
51 I. Arrnentano, N. Bitinis, E. Fortunati, S. Mattioli, N. Rescignano, R. Verdejo, M. A. Lopez-Manchado and J. M. Kenny, *Prog. Polym. Sci.*, 2013, **38**, 1720–1747.
52 M. C. Chen, Y. C. Sun and Y. H. Chen, *Acta Biomater.*, 2013, **9**, 5562–5572.
53 I. Jun, S. Jeong and H. Shin, *Biomaterials*, 2009, **30**, 2038–2047.
54 A. Kotwal and C. E. Schmidt, *Biomaterials*, 2001, **22**, 1055–1064.